INSTITUTE OF PHYSICS PUBLISHING JOURNAL OF PHYSICS A: MATHEMATICAL AND GENERAL

J. Phys. A: Math. Gen. **39** (2006) 13817–13830 doi:10.1088/0305-4470/39/44/014

Electrostatic mode envelope excitations in e–p–i plasmas—application in warm pair ion plasmas with a small fraction of stationary ions

A Esfandyari-Kalejahi[1], I Kourakis[2,3], M Mehdipoor[1] and P K Shukla[3]

[1] Department of Physics, Faculty of Science, Azarbaijan University of Tarbiat Moallem, 51745-406 Tabriz, Iran
[2] Universiteit Gent, Sterrenkundig Observatorium, Krijgslaan 281, B-9000 Gent, Belgium
[3] Fakultät für Physik und Astronomie, Institut fürTheoretische Physik IV, Ruhr-Universität Bochum, D-44780 Bochum, Germany

E-mail: ra-esfandyari@azaruniv.edu, ioannis@tp4.rub.de and ps@tp4.rub.de

Received 13 May 2006, in final form 6 September 2006
Published 17 October 2006
Online at stacks.iop.org/JPhysA/39/13817

Abstract

The nonlinear propagation of amplitude-modulated electrostatic wavepackets in an electron–positron–ion (e–p–i) plasma is considered, by employing a two-fluid plasma model. Considering propagation parallel to the external magnetic field, two distinct electrostatic modes are obtained, namely a quasi-thermal acoustic-like lower mode and a Langmuir-like optic-type upper one. These results equally apply in warm pair ion (e.g. fullerene) plasmas contaminated by a small fraction of stationary ions (or dust), in agreement with experimental observations and theoretical predictions in pair plasmas. Considering small yet weakly nonlinear deviations from equilibrium, and adopting a multiple-scales perturbation technique, the basic set of model equations is reduced to a nonlinear Schrödinger (NLS) equation for the slowly varying electric field perturbation amplitude. The analysis reveals that the lower (acoustic) mode is mostly stable for large wavelengths, and may propagate in the form of a dark-type envelope soliton (a void) modulating a carrier wavepacket, while the upper linear mode is intrinsically unstable, and thus favours the formation of bright-type envelope soliton (pulse) modulated wavepackets. The stability (instability) range for the acoustic (Langmuir-like optic) mode shifts to larger wavenumbers as the positive-to-negative ion temperature (density) ratio increases. These results may be of relevance in astrophysical contexts, where e–p–i plasmas are encountered, and may also serve as prediction of the behaviour of doped (or dust-contaminated) fullerene plasmas, in the laboratory.

PACS numbers: 52.30.Ex, 52.27.Ep, 52.35.Fp, 52.35.Mw

1. Introduction

A great deal of research effort has recently been devoted to pair plasmas, i.e. large ensembles of charged matter consisting of equal mass and opposite charge sign particles. In contrast to ordinary (electron–ion, e–i) plasmas, where the large mass difference between particle species imposes distinct frequency scales, the positively and negatively charged particles in pair plasmas respond on the same scale. Nevertheless, the characteristics of waves cannot always be deduced from what is obtained from e–i plasmas by simply letting particle masses to be equal to one-another. For instance, it is known that parallel propagating linear electromagnetic waves are not circularly but linearly polarized in pair plasmas, and Faraday rotation is absent in this case [1]. Furthermore, ion-acoustic waves have no counterpart in electron–positron (e–p) plasmas, where the electrostatic wave dispersion is of high frequency Langmuir type [2, 3]. The properties of e–p plasmas have been investigated by several authors [4–7]. Recently, the production of pair fullerene-ion plasmas in laboratory [8–10] has enabled experimental studies of pair plasmas rid of intrinsic problems involved in electron–positron plasmas, namely pair recombination processes and strong Landau damping.

In real, e.g. astrophysical contexts, e–p plasmas are also characterized by the presence of positive ions, in addition to electrons and positrons. Electron–positron–ion (e–p–i) plasmas appear in the early universe [11], active galactic nuclei [12] and in pulsar magnetospheres [13]. Furthermore, e–p–i plasmas can be created in laboratory plasmas [14–17]. The standard description of e–p–i plasmas adopted here considers fully ionized plasmas which consist of two populations of different charge signs possessing equal masses and absolute charge values ($m_1 = m_2 = m_e$, $q_1 = -q_2 = +e$), in addition to a population of positively charged ions ($m_3 = M$, $q_3 = +Z_3 e$); see for instance [18–22]. On the other hand, one may anticipate the injection of a small fraction of charged massive particles (an ion species, or dust particulates) into fullerene pair-ion plasma [8–10] (doping) in order to produce three-component plasmas which may accommodate new physical phenomena.

As far as electrostatic (ES) plasma modes [23, 24] are concerned, the occurrence and properties of nonlinear ES waves in e–p–i *plasmas* have been investigated by several authors. From a theoretical point of view, e–p–i plasmas are characterized by new, modified properties and conditions for the existence of arbitrary amplitude localized ES nonlinear excitations (which are typically modelled via the Sagdeev pseudopotential formalism [25–28]). Furthermore, small amplitude-modulated wavepackets, generically related to nonlinear Schrödinger theories [29], may be investigated via a (Krylov–Bogoliubov–Mitropolsky) reductive perturbation technique [30–32]. The nonlinear modulation of such ion-acoustic ES wavepackets was indeed studied by Salahuddin *et al* [33] in e–p–i plasmas, by considering (low-frequency) ion-acoustic oscillations against a Maxwellian background of thermalized electrons and positrons. Here, we aim at investigating the opposite edge of the ES frequency range, namely high-frequency oscillations of (light mass) electrons and positrons (or pair ions) against a neutralizing background of (heavier) ions which, given the frequency range of interest, may be considered to be immobile. A similar study with respect to pure (two-component) pair plasmas was carried out in [34, 35].

The present study is devoted to an investigation of the nonlinear amplitude modulation of electrostatic modes propagating parallel to the external magnetic field, in e–p–i plasmas. The model readily applies in pair-ion (e.g. fullerene) plasmas contaminated by a small fraction of uniform and stationary (heavier) positive ions (or, say, dust particulates). The two electron and positron (or pair ion) fluids are assumed to be warm and have a similar (yet not necessarily equal) temperature, while the neutralizing background ions are stationary. Positive background ions are implicitly considered here, although the formalism may also apply for negative ions

(e.g. dust particles) as well. Relying on a two-fluid plasma description and adopting a slowly varying amplitude hypothesis, we shall employ a multiple-scale technique [30–32] in order to derive a nonlinear Schrödinger-(NLS) type evolution equation [29] for the amplitude of weakly nonlinear electrostatic perturbations from equilibrium. The amplitude's (modulational) stability will then be studied, and the occurrence of modulated envelope excitations will be discussed. Also, the influence of the value of positron-to-electron (or positive-to-negative particle) density and temperature ratios on the modulational stability profile of ES waves will be elucidated.

The layout of this paper is as follows. In section 2, the analytical model is introduced and then employed, in section 3, as the basis of a perturbative analysis, by introducing appropriate slow space and time evolution scales. An NLS-type equation is derived, governing the (slow) amplitude evolution in time and space. The stability analysis and associated expressions for envelope soliton solutions of the NLSE are outlined in section 4. Section 5 is devoted to a discussion of the linear stability of ES waves by means of a numerical investigation of relevant quantities (NLSE coefficients). Finally, our conclusions are summarized in section 6.

2. The model equations

We shall consider a three-component plasma consisting of two inertial species, say 1 and 2, which have equal masses and equal absolute charges of the opposite sign, i.e. $q_1 = -q_2 = +Ze$, $m_1 = m_2 = m$ and a third species, say 3, having a constant density n_3, particle mass $m_3 \neq m$ and particle charge $Z_3 e \neq Ze$. In specific, this picture applies to e–p–i plasmas, for $Z = 1$, or in pair-ion (e.g. fullerene) [8–10], for $Z = 1$, 'doped' by the injection of a third charged particle species of higher mass.

The two-fluid plasma-dynamical (moment) equations for our three-component plasma include the two density (continuity) equations

$$\frac{\partial n_\alpha}{\partial t} + \vec{\nabla} \cdot (n_\alpha \vec{U}_\alpha) = 0, \tag{1}$$

and the two momentum equations

$$\frac{\partial \vec{U}_\alpha}{\partial t} + (\vec{U}_\alpha \cdot \vec{\nabla})\vec{U}_\alpha = -\frac{q_\alpha}{m_\alpha}\vec{\nabla}\phi - \frac{\vec{\nabla} p_\alpha}{m_\alpha n_\alpha}, \tag{2}$$

where the subscript α denotes either species 1 (i.e. the positive ions, or positrons) for $\alpha = +$, or species 2 (i.e. the negative ions, or electrons) for $\alpha = -$. The moment variables n_α, $\vec{U}_\alpha$ and p_α denote the density, fluid velocity and pressure of species α, respectively. The Lorentz force term is neglected, since wave propagation parallel to external magnetic field is assumed. The electric field is provided by the electric potential φ, which obeys Poisson's equation:

$$\nabla^2 \varphi = 4\pi e Z(n_- - n_+) - 4\pi Z_3 e n_3. \tag{3}$$

The background ion density n_3 is constant. The right-hand side on equation (3) is assumed to cancel at equilibrium, due to the quasi-neutrality condition $Z(n_{-,0} - n_{+,0}) - Z_3 n_3 = 0$. The system of equations (1) to (3) is closed by assuming an explicit density dependence of the pressure in the form $p_\alpha = C n_\alpha^\gamma$, where γ is the ratio of specific heats. Combining this assumption with the equation of state (at equilibrium) $p_{\alpha,0} = n_{\alpha,0} k_B T_\alpha$ (where T_α denotes the temperature of species α; k_B is Bolztmann's constant), the pressure term may be rearranged as $\vec{\nabla} p_\alpha / n_\alpha = \gamma K_B T_\alpha n_{\alpha 0}^{1-\gamma} n_\alpha^{\gamma-2} \vec{\nabla} n_\alpha$.

The model equations may be cast into a reduced (dimensionless) form by scaling the time and space variables as $t' \equiv \omega_{p,-} t$ and $x' \equiv x/\lambda_{D,-}$, respectively. We have defined the plasma

frequency $\omega_{p,\alpha} = \left(4\pi n_0 q_\alpha^2/m\right)^{1/2}$ (see that $\omega_{p,-} = \omega_{p,+} = \omega_p$ if $n_{+,0} = n_{-,0}$, only) and the Debye length $\lambda_{D,\alpha} = \left(K_B T_\alpha/m\,\omega_{p,\alpha}^2\right)^{1/2}$ (for $\alpha = +, -$). The density, velocity and electric potential state variables are scaled as $n'_\alpha = n_\alpha/n_{-,0}$, $u'_\alpha = u_\alpha/c_s$ and $\varphi' = \varphi/\varphi_0$, respectively, where we have defined the characteristic (sound) speed $c_s = (k_B T_-/m)^{1/2}$ (for negative ions) and the characteristic potential scale $\varphi_0 = K_B T_-/Ze$ (the primes will be dropped for simplicity). Combining these definitions and considering a one-dimensional geometry (along x), the model equations reduce to

$$\frac{\partial n_\alpha}{\partial t} + \vec{\nabla}\cdot(n_\alpha \vec{U}_\alpha) = 0, \tag{4}$$

$$\frac{\partial \vec{U}_\alpha}{\partial t} + (\vec{U}_\alpha\cdot\vec{\nabla})\vec{U}_\alpha = -\alpha\vec{\nabla}\phi - \frac{\gamma T_\alpha}{T_-} n_\alpha^{\gamma-2}\vec{\nabla}n_\alpha, \tag{5}$$

and

$$\nabla^2\varphi = (n_- - n_+) - \frac{Z_3}{Z}n_3, \tag{6}$$

where $\alpha = +, -$ is used as a subscript (denoting species) *and* as a factor ($= \pm 1$), throughout this text. In equilibrium, the neutrality condition $1 - \beta - \delta(Z_3/Z) = 0$ holds. Here we have defined the parameters $\beta = n_{+0}/n_{-0}$ and $\delta = n_3/n_{-0}$. See that positively charged background ions will be implicitly considered here ($Z_3 > 0$, i.e. $\delta > 0$), although the formalism readily applies for negatively charged massive particles (e.g. dust), for $Z_3 < 0$, i.e. $\delta > 0$. We note that $\beta < 1$ for $\delta \neq 0$ (in the former case, considered in the following; the opposite holds in the negative-ion case); the case $\delta = 0$ refers to 'pure' pair plasma. The choice $\gamma = 3$ is made in the following, accounting for one-dimensional wave propagation.

3. Methodology—derivation of an amplitude evolution equation

3.1. The perturbative analysis

In order to obtain an explicit evolution equation describing the propagation of modulated EA envelopes, from the model equations (4)–(6), we shall employ the standard reductive perturbation (multiple scales) technique [30–32]. The independent variables x and t are stretched as $\xi = \varepsilon(x - \lambda t)$ and $\tau = \varepsilon^2 t$, where ε is a small (real) parameter; here, λ is a free (real) parameter, which is to be later determined as the wave's group velocity by compatibility requirements. The dependent variables are expanded as

$$n_- = 1 + \sum_{n=1}^{\infty}\sum_{l=-\infty}^{+\infty} \varepsilon^n n_{-,l}^{(n)}(\xi,\tau)\,\mathrm{e}^{\mathrm{i}l(kx-\omega t)}, \qquad n_+ = \beta + \sum_{n=1}^{\infty}\sum_{l=-\infty}^{\infty} \varepsilon^n n_{+,l}^{(n)}(\xi,\tau)\,\mathrm{e}^{\mathrm{i}l(kx-\omega t)}$$

$$U_+ = \sum_{n=1}^{\infty}\sum_{l=-\infty}^{\infty} \varepsilon^n U_{+,l}^{(n)}(\xi,\tau)\,\mathrm{e}^{\mathrm{i}l(kx-\omega t)}, \qquad U_- = \sum_{n=1}^{\infty}\sum_{l=-\infty}^{\infty} \varepsilon^n U_{-,l}^{(n)}(\xi,\tau)\,\mathrm{e}^{\mathrm{i}l(kx-\omega t)} \tag{7}$$

$$\phi = \sum_{n=1}^{\infty}\sum_{l=-\infty}^{\infty} \varepsilon^n \phi_l^{(n)}(\xi,\tau)\,\mathrm{e}^{\mathrm{i}l(kx-\omega t)}$$

where ω and k are the real parameters denoting the wave's frequency and wavenumber; the reality condition $A_{-l}^{(n)} = A_l^{(n)*}$ is met by all state variables; the star superscript denotes the complex conjugate of the (complex) harmonic amplitudes.

Substituting the expansion ansatz (7) and the stretched variables ξ, τ into equations (4)–(6), and then isolating distinct orders in ε, we obtain the nth order reduced density equation

$$-\lambda\frac{\partial n_{\alpha,l}^{(n-1)}}{\partial\xi}+\frac{\partial n_{\alpha,l}^{(n-2)}}{\partial\tau}-\mathrm{i}l\omega n_{\alpha,l}^{(n)}+\mathrm{i}lk\kappa_\alpha U_{\alpha,l}^{(n)}+\kappa_\alpha\frac{\partial U_{\alpha,l}^{(n-1)}}{\partial\xi}$$
$$+\sum_{n'=1}^{\infty}\sum_{l'=-\infty}^{\infty}\left[\mathrm{i}lkn_{\alpha,l'}^{(n')}U_{\alpha,l-l'}^{(n-n')}+\frac{\partial}{\partial\xi}\left(n_{\alpha l'}^{(n')}U_{\alpha,l-l'}^{(n-n'-1)}\right)\right]=0, \tag{8}$$

density equation

$$\frac{\partial U_{\alpha,l}^{(n-2)}}{\partial\tau}-\lambda\frac{\partial U_{\alpha,l}^{(n-1)}}{\partial\xi}-\mathrm{i}l\omega n_{\alpha,l}^{(n)}+\sum_{n'=1}^{\infty}\sum_{l'=-\infty}^{\infty}\left[\mathrm{i}l'kU_{\alpha,l-l'}^{(n-n')}U_{-,l}^{(n)}+U_{\alpha,l-l'}^{(n-n'-1)}\frac{\partial U_{\alpha,l'}^{(n')}}{\partial\xi}\right]$$
$$=-\alpha\frac{\partial\varphi_l^{(n-1)}}{\partial\xi}-\mathrm{i}l\alpha k\varphi_l^{(n)}-3\mathrm{i}lk\kappa_\alpha n_{\alpha,l}^{(n)}-3\kappa_\alpha\sigma_\alpha\frac{\partial n_{\alpha,l}^{(n-1)}}{\partial\xi}$$
$$-3\sum_{n'=1}^{\infty}\sum_{l'=-\infty}^{\infty}\left[\mathrm{i}l'n_{\alpha,l-l'}^{(n-n')}kn_{-,l'}^{(n')}+n_{\alpha,l-l'}^{(n-n'-1)}\frac{\partial n_{\alpha,l'}^{(n')}}{\partial\xi}\right], \tag{9}$$

and Poisson's equation

$$\frac{\partial^2\varphi_l^{(n-2)}}{\partial\xi^2}-l^2k^2\varphi_l^{(n)}+2\mathrm{i}lk\frac{\partial\varphi_l^{(n-1)}}{\partial\xi}=n_{-,l}^{(n)}-n_{+,l}^{(n)} \tag{10}$$

where $\sigma_\alpha=T_\alpha/T_-$, i.e. $\sigma_-=1$ and $\sigma_+=\sigma=T_+/T_-$; and $\kappa_\alpha=1$ for $\alpha=-$ and $\kappa_\alpha=\beta$ for $\alpha=+$; recall that $\beta=n_{+,0}/n_{-,0}$.

From the first-order ($n=1$) equations, we obtain

$$\begin{aligned}
&-\mathrm{i}l\omega n_{-,l}^{(1)}+\mathrm{i}lkU_{-,l}^{(1)}=0, && -\mathrm{i}l\omega n_{+,l}^{(1)}+\mathrm{i}lk\beta U_{+,l}^{(1)}=0\\
&-\mathrm{i}l\omega U_{-,l}^{(1)}=\mathrm{i}lk\varphi_l^{(1)}-3\mathrm{i}lkn_{-,l}^{(1)}, && -\mathrm{i}l\omega U_{+,l}^{(1)}=-\mathrm{i}lk\varphi_1^{(1)}-3\mathrm{i}l\sigma k\beta n_{+,1}^{(1)},\\
&-l^2k^2\phi_l^{(1)}=n_{-,l}^{(1)}-n_{+,l}^{(1)},
\end{aligned} \tag{11}$$

from which the following dispersion relation is deduced, for $l=1$

$$\frac{\beta}{\omega^2-3\sigma k^2\beta^2}+\frac{1}{\omega^2-3k^2}=1, \tag{12}$$

as a compatibility requirement. Two real solutions are thus obtained for the frequency square ω^2, defined by

$$\omega_1^2=\frac{1+\beta}{2}+\frac{3}{2}(1+\sigma\beta^2)k^2-\frac{1}{2}\sqrt{9k^4(1-\sigma\beta)^2+6(\beta-1)(\sigma\beta^2-1)k^2+(1+\beta)^2} \tag{13a}$$

and

$$\omega_2^2=\frac{1+\beta}{2}+\frac{3}{2}(1+\sigma\beta^2)k^2+\frac{1}{2}\sqrt{9k^4(1-\sigma\beta)^2+6(\beta-1)(\sigma\beta^2-1)k^2+(1+\beta)^2}. \tag{13b}$$

See that, for all values of β and σ, the lower mode satisfies $\omega_1\to 0$ as $k\to 0$, while the upper mode goes to a finite cutoff frequency $\omega_1\to\sqrt{1+\beta}$, as observed in the experiment by Oohara and Hatakeyama [10].

For small k, these branches behave as

$$\omega_1^2\approx 3\beta(1+\sigma\beta)k^2/(1+\beta), \tag{14a}$$

and

$$\omega_2^2\approx 1+\beta+3(1+\sigma\beta^3)k^2/(1+\beta), \tag{14b}$$

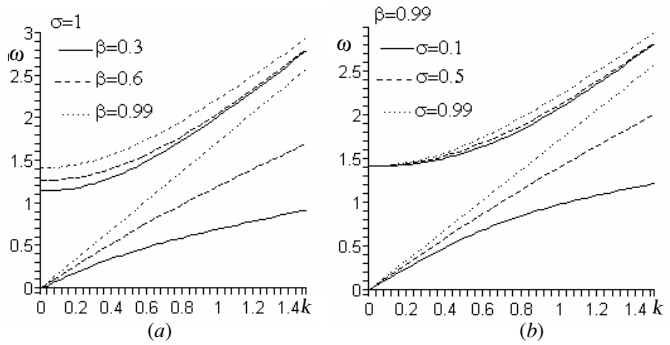

Figure 1. The two dispersion curves defined by equation (13) are depicted, as a frequency ω/ω_p variation versus the reduced wavenumber $k\lambda_D$.

i.e. recovering dimensions,

$$\omega_1^2 \approx 3\beta(1+\sigma\beta)c_s k^2/(1+\beta)$$

and

$$\omega_2^2 \approx (1+\beta)\omega_p^2 + 3(1+\sigma\beta^3)c_s^2 k^2/(1+\beta)$$

(setting $\beta = \sigma = 1$, one recovers the pure pair plasma limit formulae which is found in the literature). See that the cutoff frequency $\omega_1 \to \omega_p\sqrt{1+\beta}$ is affected by the pair-species' densities, but not by their temperatures; cf figures 1(*a*) and (*b*). Two characteristic velocities, $c_{0L} = c_s\sqrt{3\beta(1+\sigma\beta)/(1+\beta)}$ and $c_{0U} = c_s\sqrt{3(1+\sigma\beta^3)/(1+\beta)}$ are thus defined. Electrostatic modes in e–p–i plasmas therefore include an *acoustic* dispersion, $\omega_1 \approx \pm c_{oL}k$, and a Langmuir-like optical behaviour $\omega_2 \approx \pm\sqrt{(1+\beta)\omega_p^2 + c_{0U}^2k^2}$, for small k. For clarity, $\omega_1 = \omega_L$ and $\omega_2 = \omega_U$ will henceforth be referred to as the lower and the upper curve, respectively. Note, for rigour, that the lower branch has been argued to be subject to strong damping, in electron–positron plasmas, due to the phase velocity ω_1/k being close to the sound velocity [36]. However, this may not necessarily be true in e–p–i , thanks to the extra ion component and/or the pair-ion species temperature ratio, which affects the wave front phase velocity. The dispersion laws presented here are in full agreement with (and, in fact, generalize) known experimental [8, 9] and theoretical [3] results for pair plasmas. It may be noted, for the sake of rigor, that the lower dispersion relation cannot exist for an identical positive and negative ion population plasma preparation to see this, set $\beta = \sigma = 1$ in equation (12), a fact which seems to point towards an asymmetry of the pair-ion constituents in the experiment described in [8, 9] (where the acoustic mode was indeed observed).

The two dispersion curves obtained above are depicted in figure 1. We note on the plots the dependence of the dispersion relation on the parameters involved, namely the positive-to-negative ion (or positron-to-electron) density and temperature ratios β and σ. The wave frequency for a fixed wavenumber clearly increases with higher β, i.e. for a lower fixed ion concentration; in other words, the addition of a stationary positive ion component results in lower frequency values and lower phase speeds, for small k; the phase velocity (slope) is also affected—see in figure 1(*a*). The opposite effect should be expected if the stationary ions were negatively charged. On the other hand, higher values of the temperature σ (e.g. hotter positrons, in e–p–i plasma) result in lower frequency values—see in figure 1(*b*). All of these effects are more intense in the lower (acoustic) mode, and only slightly observed in the upper

mode (hence the extreme parameter values considered in figure 1, to depict the change in the curve).

The first-order first harmonic amplitudes are now determined as

$$\begin{aligned} n^{(1)}_{-,1} &= \frac{k^2}{-\omega^2+3k^2}\varphi^{(1)}_1, \qquad n^{(1)}_{+,1} = \frac{k^2\beta}{\omega^2-3\sigma k^2\beta^2}\varphi^{(1)}_1, \qquad k\beta U^{(1)}_{+,1} = \omega n^{(1)}_{+,1}, \\ U^{(1)}_{-,l} &= \frac{k\omega}{-\omega^2+3k^2}\varphi^{(1)}_1, \qquad U^{(1)}_{+,1} = \frac{k\omega}{\omega^2-3\sigma k^2\beta^2}\varphi^{(1)}_1. \end{aligned} \tag{15}$$

The frequency in these (and all forthcoming) expressions refers to either the lower or the upper branch. Note that these expressions would be meaningless if $\sigma = 1$ and $\beta = 1$ were simultaneously satisfied the denominators would then vanish; cf (13*a*) and (13*b*)); this is not the case here, by assumption.

For the second-order ($n = 2$) equations with $l = 1$ (first harmonics), we deduce the following compatibility condition:

$$\lambda = \frac{\omega}{k} - \frac{1}{k\omega\left[\frac{1}{(\omega^2-3k^2)^2} + \frac{\beta}{(\omega^2-3\sigma k^2\beta^2)^2}\right]}. \tag{16}$$

It is easy to show that $\lambda = v_g(k) = \partial\omega/\partial k$. The real parameter λ therefore denotes the group velocity.

3.2. The nonlinear Schrödinger equation

Proceeding to $n = 2, l = 2$ in combination with $n = 3, 1 = 0, 1$ in equations (8)–(10), we obtain a compatibility condition in the form of the nonlinear Schrödinger equation:

$$\mathrm{i}\frac{\partial\varphi}{\partial\tau} + P\frac{\partial^2\varphi}{\partial\xi^2} + Q\,|\varphi|^2\,\varphi = 0, \tag{17}$$

which describes the slow evolution of the first-order amplitude of the plasma potential perturbation $\varphi \equiv \varphi^{(1)}_1$. The dispersion coefficient P is related to the dispersion curve as $P = \partial^2\omega/2\partial k^2$. Its exact form reads

$$\begin{aligned} P = {} & \frac{(\omega^2-k\lambda\omega)^2(\omega-k\omega)}{2\omega^2k^2}\left[\frac{\omega^2+3k^2}{(\omega^2-3k^2)^3} + \frac{\beta(\omega^2+3\sigma k^2\beta^2)}{(\omega^2-3\sigma k^2\beta^2)^3}\right] \\ & + \frac{3(\omega^2-k\lambda\omega)^2}{\omega}\left[\frac{1}{(\omega^2-3k^2)^3} + \frac{\sigma\beta^3}{(\omega^2-3\sigma k^2\beta^2)^3}\right] - \frac{\omega^2-k\lambda\omega}{2\omega k^2} \\ & - \frac{(\omega^2-k\lambda\omega)^2\lambda}{k}\left[\frac{1}{(\omega^2-3k^2)^3} + \frac{\beta}{(\omega^2-3\sigma k^2\beta^2)^3}\right]. \end{aligned} \tag{18}$$

The nonlinearity coefficient Q, which is due to the carrier wave self-interaction, is given by

$$\begin{aligned} Q = {} & -\frac{k^3(2\omega+k\lambda)(\omega^2-k\lambda\omega)}{2\lambda\omega}\left[\frac{(\omega^2+3k^2)}{(\omega^2-3k^2)^4} + \frac{\beta(\omega^2+3\sigma k^2\beta^2)}{(\omega^2-3\sigma k^2\beta^2)^4}\right] \\ & - \frac{3k^4(\omega^2-k\lambda\omega)}{4\omega}\left[\frac{(\omega^2+3k^2)(\omega^2+k^2)}{(\omega^2-3k^2)^5} + \frac{\beta(\omega^2+3\sigma k^2\beta^2)(\omega^2+\sigma k^2\beta^2)}{(\omega^2-3\sigma k^2\beta^2)^5}\right] \\ & - \frac{3k^4(\omega^2-k\lambda\omega)}{4\omega}\left[\frac{(\omega^2+k^2)[\omega^2+k^2+6k^2(\omega^2-3k^2)]}{(\omega^2-3k^2)^6}\right. \\ & \left. + \frac{\beta^2(\omega^2+\sigma k^2\beta^2)[\omega^2+\sigma k^2\beta^2+6\sigma k^2\beta(\omega^2-3\sigma k^2\beta^2)]}{(\omega^2-3\sigma k^2\beta^2)^6}\right] \end{aligned}$$

$$+\frac{3\beta k^4(\omega^2+k^2)(\omega^2+\sigma k^2\beta^2)(\omega^2-k\lambda\omega)}{2\omega(\omega^2-3k^2)^3(\omega^2-3\sigma k^2\beta^2)^3}+\frac{(2k\lambda\omega+\omega^2+3k^2)(\omega^2-k\lambda\omega)}{2\omega[\lambda^2-3\sigma\beta^2+(\lambda^2-3)\beta]}$$
$$\times\left[\frac{2\omega k^3(\lambda^2-3\sigma\beta^2-3\beta)-k^2\beta\lambda(\omega^2+3k^2)}{\lambda(\omega^2-3k^2)^4}-\frac{4\omega k^3\lambda\beta}{(\omega^2-3k^2)^2(\omega^2-3\sigma k^2\beta^2)^2}\right.$$
$$-\frac{k^2\beta(2\omega^2+3k^2+3\sigma k^2\beta^2)}{(\omega^2-3k^2)^2(\omega^2-3\sigma k^2\beta^2)^2}$$
$$\left.+\frac{2\omega k^3\beta^2(\lambda^2-3\sigma\beta-3)-k^2\beta\lambda(\omega^2+3\sigma k^2\beta^2)}{\lambda(\omega^2-3\sigma k^2\beta^2)^4}\right]. \tag{19}$$

It may be interesting to trace the asymptotic behaviour of these coefficients for small k, i.e. for a large wavelength, compared to the Debye radius. At first we consider low mode. P_L behaves as $P_L \approx -c_{P,L}k$ for small k, while Q_L goes to infinity as $Q_L \approx c_{Q,L}/k$ (the expressions for the quantities $c_{P,L}$ and $c_{Q,L}$ are given in the appendix). The product PQ is therefore negative (prescribing modulational stability, as we shall see) and independent of k, for small k (i.e. in the long-wavelength limit), while $P/Q \propto -k^2$ in the same limit. For the upper mode, P_U goes to a constant as $P_U \sim 3(\sigma^3+1)/(1+\beta)^{3/2} > 0$, while Q_U behaves as $Q_U \sim c_{Q,U}k^2 > 0$ (the expression for $c_{Q,U}$ is given in the appendix). The product PQ is therefore positive (favouring modulational instability, as we will see below) and tends to zero, for small k, while $P/Q \sim k^{-2} > 0$ in the same limit.

4. Modulational instability and envelope excitations

4.1. Modulational stability analysis

The stability analysis of the NLS equation (17) consists in linearizing around the monochromatic wave solution $\psi = \hat{\psi}\,\mathrm{e}^{\mathrm{i}Q|\hat{\psi}|^2\tau}$, i.e. by setting $\hat{\psi} = \hat{\psi}_0 + \varepsilon\hat{\psi}_1$, and then taking the perturbation $\hat{\psi}_1$ to be of the form $\hat{\psi}_1 = \hat{\psi}_{1,0}\,\mathrm{e}^{\mathrm{i}(\hat{k}\xi-\hat{\omega}\tau)}$ (the perturbation wavenumber $\hat{k}$ and frequency $\hat{\omega}$ should be distinguished from the carrier wave quantities k and ω). One thus obtains the dispersion relation $\hat{\omega}^2 = P\hat{k}^2(P\hat{k}^2 - 2Q|\hat{\psi}_0|^2)$. In order for the wave to be stable, the product PQ must be negative. Otherwise, for positive PQ, instability sets in for perturbation wavenumber values below a critical value $\hat{k}_{cr} = \sqrt{2Q/P}|\hat{\psi}_0|$, i.e. for wavelength values above the threshold $\lambda_{cr} = 2\pi/\hat{k}_{cr}$. The maximum instability growth rate $\sigma = |\mathrm{Im}\,\hat{\omega}(\hat{k})|$, i.e. $\sigma_{\max} = |\mathrm{Im}\,\hat{\omega}|_{\hat{k}=\hat{k}_{cr}/\sqrt{2}} = |Q||\hat{\psi}_0|^2$, is achieved for $\hat{k} = \hat{k}_{cr}/\sqrt{2}$.

We draw the conclusion that the instability condition depends only on the sign of the product PQ, which may be studied numerically, relying on the exact expressions derived above.

4.2. Envelope soliton solutions of the NLSE

The localized solutions of the NLSE (17) describe (arbitrary amplitude) nonlinear excitations, in the form of bright and dark (black/grey) envelope solitons. Exact expressions for these envelope structures can be found by substituting with $\varphi = \sqrt{\rho}\exp(i\theta)$ into equation (17), and then separating real and imaginary parts. The final formulae are exposed e.g. in [32, 37], and will therefore only briefly be summarized in the following.

For $PQ > 0$ we find the *bright* envelope soliton:

$$\rho = \rho_0\,\mathrm{sech}^2\left(\frac{\xi-u\tau}{l}\right), \qquad \theta = \frac{1}{2P}\left[u\xi-\left(\Omega+\frac{1}{2}u^2\right)\tau\right]$$

which represents a localized pulse travelling at a speed u and oscillating at a frequency

Ω (at rest). The pulse width l depends on the constant maximum amplitude square ρ_0 as $l = \sqrt{2P/Q\rho_0}$. We note that the maximum amplitude $\sqrt{\rho_0}$ is inversely proportional to the spatial extension l; this is in fact also true in the dark (i.e. black/grey) envelope soliton case (see below).

For $PQ < 0$ we have the *black* envelope soliton

$$\rho = \rho_1 \left[1 - \operatorname{sech}^2 \left(\frac{\xi - u\tau}{l'} \right) \right] = \rho_1 \tanh^2 \left(\frac{\xi - u\tau}{l'} \right),$$
$$\theta = \frac{1}{2P} \left[u\xi - \left(\frac{1}{2}u^2 - 2PQ\rho_1^2 \right) \tau \right],$$

representing a localized region of negative wave density travelling speed u. The pulse width depends on the maximum amplitude square ρ_1 via $l' = \sqrt{|2P/Q\rho_1|}$.

Finally, for $PQ < 0$, one also obtains the *grey envelope soliton* excitation

$$\rho = \rho_2 \left[1 - a^2 \operatorname{sech}^2 \left(\frac{\xi - u\tau}{l''} \right) \right],$$

which also represents a localized region of negative wave density, θ_{10} is a constant phase, s denotes the product $s = \text{sign}\, P \times \text{sign}(u - V_0)$. In comparison to the *black* soliton above, note that apart from the maximum amplitude $\sqrt{\rho_2}$, which is now finite everywhere, the pulse width of this grey-type excitation: $l'' = (1/a)\sqrt{2|P/Q\rho_2|}$, now also depends on the dimensionless parameter a, which is given by $a^2 = 1 + (u - V_0)^2/(2PQ\rho_2) \leqslant 1$ (for $PQ < 0$), an independent parameter representing the modulation depth ($0 < a \leqslant 1$). V_0 is an independent real constant which satisfies the condition: $V_0 - \sqrt{2|PQ|\rho_2^2} \leqslant u \leqslant V_0 + \sqrt{2|PQ|\rho_{2^2}}$; for $V_0 = u$, we have $a = 1$ and thus recover the *black* soliton presented in the previous paragraph.

5. Numerical analysis

Summarizing the previous section, we have seen that the sign of the coefficient product PQ determines the stability profile of ES waves and the type of envelope excitations (negative/positive for stability/instability and bright/dark type envelope solitons), while the ratio P/Q determines the spatial extension of the localized envelope structures for a given maximum amplitude (and vice versa), in an inverse-proportional manner. We may now investigate the numerical value of these quantities in terms of the relevant physical parameters, namely the positron-to-electron (or positive-to-negative ion) density and temperature ratio(s), $\beta = n_{+,0}/n_{-,0}$ and $\sigma_+ = \sigma = T_+/T_-$, respectively.

The results of the calculations for fixed values of σ and different values of β for the lower mode (acoustic branch) are shown in figures 2(*a*) and (*b*), for small k (large wavelengths), and in figures 3(*a*) and (*b*) for higher k. We may nevertheless admit, for rigor, that figures 3(*a*) and (*b*) are invalidated by Landau damping, which is expected to be dominant for large k (where the ES wave phase velocity is comparable to the ion thermal velocity), and are thus only provided for indicative purposes. We find out that both dark (grey or black, for $PQ < 0$) and bright (for $PQ > 0$) excitations may occur. The former dominate the large wavelength (small k) region, while the latter exist in a bounded range of values for shorter wavelengths in which $PQ > 0$ (namely, from a zero-nonlinearity point $k = k_{\text{ZNP}} > 0$, where $Q = 0$ or $P/Q \to \pm\infty$, up to a zero-dispersion point, $k = k_{\text{ZDP}}$, say ZDP, where $P = 0$). Upon careful inspection of figure 2(*a*) and figure 3(*a*), one observes that the range of positive PQ values (hence instability) increases and shifts to higher values of k as β increases, for a fixed σ. As figure 2(*b*) shows, the width of grey and dark excitations increases as k increases until $k = k_{\text{ZNP}}$, while that of bright excitations decreases as k increases from $k = k_{\text{ZNP}}$ up to $k = k_{\text{ZDP}}$. For a fixed value of

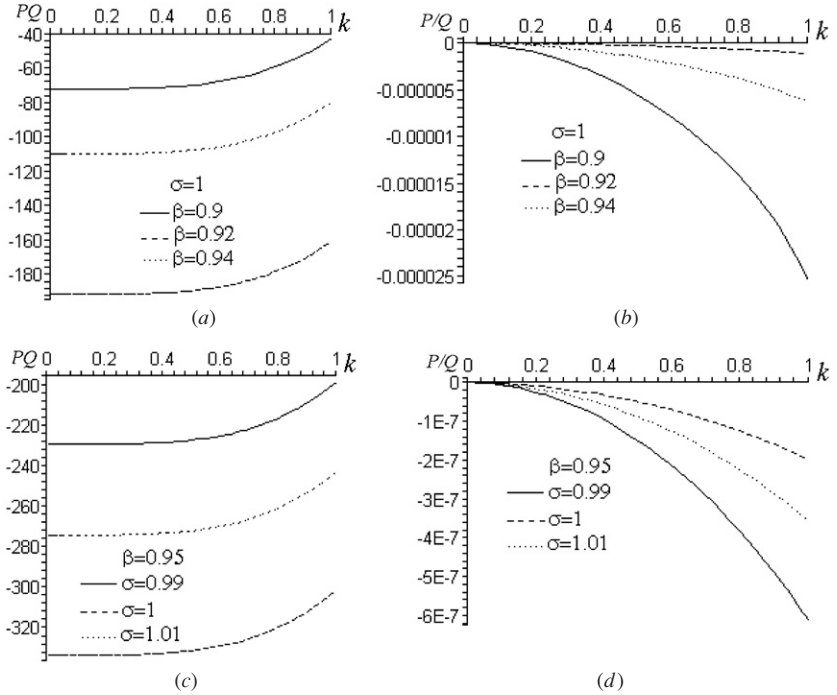

Figure 2. The NLSE coefficient product PQ ((*a*) and (*c*)) and ratio P/Q ((*b*) and (*d*)) corresponding to the lower dispersion branch ω_1 are depicted against the reduced wavenumber $k\lambda_D$ (in abscissa everywhere). Here ((*a*) and (*b*)) $\sigma = 1$, and different values of β are considered; ((*c*) and (*d*)) $\beta = 0.95$, and σ varies.

k, the width of dark (bright) excitations is shown to decrease (increase), for a given maximum amplitude, as the density ratio increases. Admittedly, as stated above, high values of k are rather excluded physically, due to Landau damping (which is inevitably omitted in a fluid plasma description), so we need not pursue this analysis any further. Also, we note that the NLSE-based analysis breaks down near the ZDP, where higher-order nonlinearity takes over (this is a well-known phenomenon in nonlinear optics).

Considering a fixed value of β for different values of σ, for the lower mode, we have obtained figures 2(*c*) and (*d*) and figure 3(*c*) and (*d*). The qualitative aspects of the above analysis are also valid in this case. Thus, increasing the density of positrons (or positive ions) with respect to their electron (or negative ion) counterpart results in an increase in the wavenumber instability threshold, and therefore slightly favours stability. For a fixed value of k, the width of dark (bright) excitations is shown to decrease (increase), for a given maximum amplitude, as the temperature ratio increases.

Let us consider the upper mode (optical dispersion branch). The results of the calculation for a fixed temperature ratio σ and different values of the density ratio β (or, respectively, fixed β and varying σ) for this mode are shown in figures 4(*a*) and (*b*) (or, respectively, figures 4(*c*) and (*d*)). Both dark (for $PQ < 0$) and bright (for $PQ > 0$) excitations can exist for this mode. Note, however, that the qualitative profile is reversed, with respect to the lower mode: here, bright excitations and modulational instability occur for small k, in fact from zero up to a threshold $k = k_{cr}$ (see that $Q \to \pm\infty$ as $k \to k_{cr}$), while dark excitations (and modulational stability of the envelope) occur for larger k, after $k = k_{cr}$. As the width of bright

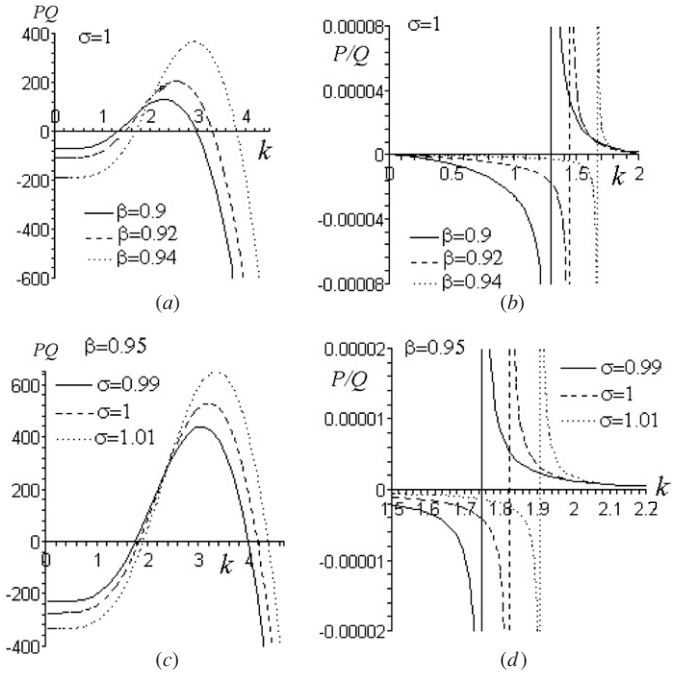

Figure 3. The same as in figure 2, for higher wavenumber k values.

excitations becomes narrower as k increases from zero up to $k = k_{cr}$, where it reaches zero. Beyond $k = k_{cr}$, only stable envelopes may propagate, in the form of dark-type envelope solitons; the corresponding localized envelope width increases up to a maximum value, and then decreases as k increases (still, these low wavelength results are to be interpreted with precaution). Upon careful inspection of figures 3(a) and (c), one observes that k_{cr} shifts to larger values as either σ or β increases.

Summarizing, we conclude that the lower (acoustic) mode is generally stable, for realistic large wavelength situations (see figures 2(a) and (d)) and may propagate in the form of a dark-type envelope soliton (i.e. a potential dip, a void). On the other hand, the upper (Langmuir-like) mode is modulationally unstable (see figures 4(a) and (d)), and may favour the formation of bright-type envelope soliton (pulse) modulated wavepackets at low wavenumbers. We remark that, once the potential perturbation is determined by the NLSE (17), the density and velocity variations are given by expressions (15); it may be checked that the two fluids (negative and positive ions) are subject to a perturbation of opposite sign to one-another: an increase in the number density (or the velocity) of one entails a depletion (or a slow-down) in the other, as may be seen in equation (15). Finally, comparing to the 'pure' e–p (or pair–ion) plasma, which was presented in [34, 35], we note that the qualitative profile depicted above remains similar (despite an analytical complication discussed in [35]). It should be pointed out, however, that all relevant wavenumber thresholds are increased in our case here; this implies that the presence of ions in e–p plasma (respectively: charged defects, say, in pair-ion plasma) results in a significant increase of the wavenumber range where the lower (acoustic) mode is stable (favouring dark solitons, i.e. holes/voids) and/or where the upper (Langmuir-like) mode is unstable (favouring bright solitons, i.e. pulses).

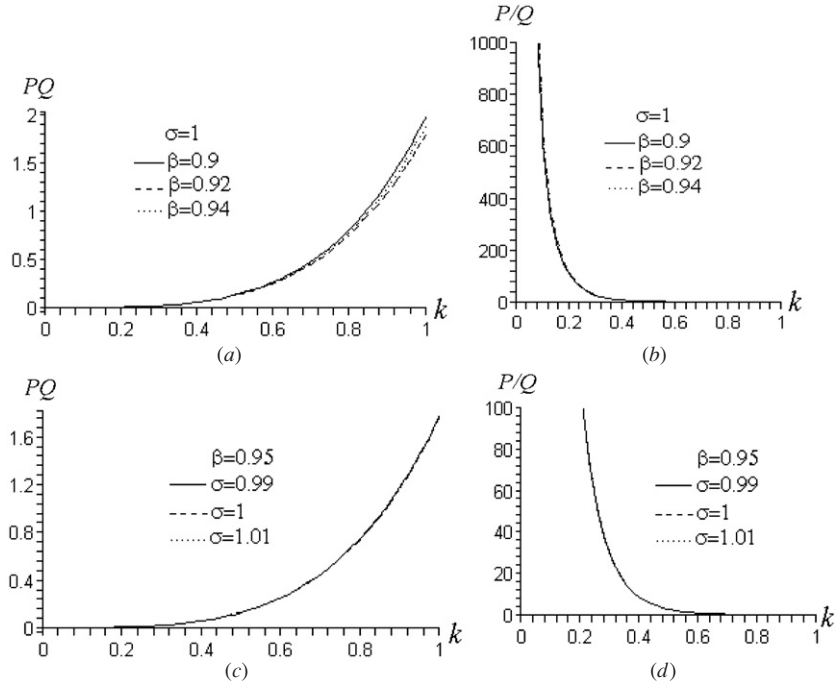

Figure 4. The NLSE coefficient product PQ ((*a*) and (*c*)) and the ratio P/Q ((*b*) and (*d*)) corresponding to the lower dispersion branch ω_2 are depicted against the reduced wavenumber $k\lambda_D$ (in abscissa everywhere). Here ((*a*) and (*b*)) $\sigma = 1$, and different values of β are considered; ((*c*) and (*d*)) $\beta = 0.95$, and σ varies.

6. Conclusions

In this paper, we have investigated the nonlinear propagation of electrostatic wavepackets in e–p–i plasmas, by employing a two-fluid plasma model. The results equally apply in the case of a pair-ion plasma, in the presence of a small fraction of uniform and stationary charged particles (e.g. dust). Electrostatic mode propagation parallel to the external magnetic field was considered. The temperature ratio between the two species has been left arbitrary in the analysis, although a natural choice of unity was implicitly focused upon. Two distinct electrostatic modes were obtained, namely a quasi-thermal lower mode and a Langmuir-like optic-type upper one which is the case for pure pair plasmas, in agreement with previous experimental observations confirmed by theoretical studies of equal-temperature pair plasmas. Considering small yet weakly nonlinear deviations from equilibrium, and adopting a multiple scale technique, the basic set of model equations was reduced to a nonlinear Schrödinger equation for the slowly varying electric field perturbation amplitude.

The analysis revealed that the stability range of lower (acoustic) mode increases as the positive ion (or positron) to negative ion (or electron) ion density ratio β increases. The lower mode may propagate in the form of a dark-type envelope soliton (i.e. a potential dip, or a void) which modulates a carrier wave. On the other hand, the upper mode is mostly modulationally unstable, and may yet favour the formation of bright-type envelope soliton (pulse) modulated wavepackets at small wavenumbers. As mentioned above, these results depend on the temperature ratio, as one may see in figures 2–4. In specific, one may anticipate

that a local coexistence of positive ions (or positrons) with a colder, say, population of negative ions (or electrons), namely $\sigma < 1$ ($\sigma > 1$), may critically affect the stability profile of electrostatic modes, for instance by stabilizing the lower mode, or by destabilizing the upper mode.

It should be added, for rigour, that our results on the lower mode are somewhat invalidated by Landau damping, which will dominate if the pair-ion temperatures are equal. However, we speculate that allowing for $T_+ \neq T_-$, and hence modifying the group velocity (see the slope in figure 1(*b*)) may decrease Landau damping and allow ES oscillations to survive. Preliminary theoretical calculations in this direction are currently carried out and should be reported soon.

These results are relevant to recent observations of electrostatic waves in pair-ion (fullerene) plasmas. In particular, one may anticipate doping fullerene plasmas with charged massive defects (or dust particles), in order to tune the characteristic features of plasma modes. This analysis may also be relevant to modulated electron–positron–ion plasma radio emission in pulsar magnetospheres. Our predictions may be investigated, and will hopefully be confirmed, by appropriately designed experiments.

Acknowledgments

The work of one of us (IK) was partially supported by the Deutsche Forschungsgemeinschaft (Bonn, Germany) through the Sonderforschungsbereich (SFB) 591—Universelles Verhalten Gleichgewichtsferner Plasmen: Heizung, Transport und Strukturbildung. IK wishes to thank Professor F Verheest for a number of enlightening discussions on pair plasmas. He also acknowledges the hospitality of Sterrenkundig Observatorium (Universiteit Gent, Belgium), where this work was completed. AE-K, IK and PKS gratefully acknowledge the hospitality offered by the Abdus Salam International Centre for Theoretical Physics, during the International Workshop on Frontiers of Plasma Science (August 2006), during which part of this work was carried out. The assistance offered by the anonymous referee is gratefully acknowledged.

Appendix

$$c_{P,L} = \frac{9\sqrt{3}(\sigma\beta^2-1)^2\sqrt{\frac{\beta(1+\sigma\beta)}{1+\beta}}}{2[1+(2+\sigma)\beta+(1+2\sigma)\beta^2+\sigma\beta^3]}$$

$$\begin{aligned} C_{Q,L} = \Bigg(& (9\sqrt{3}\,\sigma^2\beta^9 + 18\sqrt{3}\,\sigma^2\beta^8 + 24\sqrt{3}\,\beta^8\sigma + 54\sqrt{3}\,\beta^7\sigma + 26\sqrt{3}\,\sigma^2\beta^7 + 16\sqrt{3}\,\beta^7) \\ & + 40\sqrt{3}\,\beta^6 + 84\sqrt{3}\,\beta^6\sigma + 32\sqrt{3}\,\sigma^2\beta^6 + 65\sqrt{3}\,\beta^5 + 21\sqrt{3}\,\sigma^2\beta^5 + 116\sqrt{3}\,\beta^5\sigma \\ & + 14\sqrt{3}\,\sigma^2\beta^4 + 104\sqrt{3}\,\sigma\beta^4 + 90\sqrt{3}\,\beta^4 + 82\sqrt{3}\,\beta^3 + 8\sqrt{3}\,\sigma^2\beta^3 + 78\sqrt{3}\,\sigma\beta^3 \\ & + 56\sqrt{3}\,\beta^2 + 44\sqrt{3}\,\sigma\beta^2 + 8\sqrt{3}\,\sigma\beta + 29\sqrt{3}\,\beta + 6\sqrt{3})\sqrt{\frac{\beta(1+\sigma\beta)}{\sigma+\beta}}\Bigg) \Bigg/ \\ & (-1296\sigma^4\beta^{10} + 1944\sigma^3\beta^8 - 1296\sigma^2\beta^6 + 324\sigma^5\beta^{12} - 1296\sigma^3\beta^9 \\ & + 1944\sigma^2\beta^7 - 1296\beta^5\sigma + 324\sigma^4\beta^{11} + 324\sigma\beta^4 - 324\beta^3) \end{aligned}$$

$$\begin{aligned} C_{Q,U} = & \frac{1}{3(1+\beta)^{(29/2)}\sigma\beta + 3(1+\beta)^{(29/2)}} \\ & \times (2\beta^{13} + 26\beta^{12} + 156\beta^{11} + 572\beta^{10} + 1430\beta^9 + 2574\beta^8 \\ & + 3432\beta^7 + 3432\beta^6 + 2574\beta^5 + 1430\beta^4 + 572\beta^3 + 156\beta^2 + 26\beta + 2). \end{aligned}$$

References

[1] Chen F F 1974 *Introduction to Plasma Physics* (New York: Plenum) p 121
Hall J O and Shukla P K 2005 *Phys. Plasmas* **12** 084507
[2] Iwamoto N 1993 *Phys. Rev.* E **47** 604
[3] Zank G P and Greaves R G 1995 *Phys. Rev.* E **51** 6079
[4] Bulanov S S 2004 *Phys. Rev.* E **69** 036408
[5] Kluger Y, Eisenberg J M, Svetitsky B, Cooper F and Mottola E 1991 *Phys. Rev. Lett.* **67** 2427–30
[6] Prozorkevich A V, Reichel A, Smolyansky S A and Tarakanov A V 2004 *Proc. SPIE* **5476** 68–72
[7] Greaves R G, Tinkle M D and Surko C M 1994 *Phys. Plasmas* **1** 1439
[8] Oohara W and Hatakeyama R 2003 *Phys. Rev. Lett.* **91** 205005
[9] Oohara W, Date D and Hatakeyama R 2005 *Phys. Rev. Lett.* **95** 175003
[10] Hatakeyama R and Oohara W 2005 *Phys. Scr.* **116** 101
[11] Rees M J 1983 *The Very Early Universe* Cambridge: Cambridge University Press)
[12] Miller H R and Witta P J 1987 *Active Galactic Nuclei* (Berlin: Springer) p 202
[13] Michel F C 1982 *Rev. Mod. Phys* **54** 1
[14] Greaves R G and Surko C M 1995 *Phys. Rev. Lett.* **75** 3847
[15] Berezhiani V I, Tskhakaya D D and Shukla P K 1992 *Phys. Rev.* A **46** 6608
[16] Surko C M, Levelhal M, Crane W S, Passne A and Wysocki F 1986 *Rev. Sci. Instrum* **57** 1862
[17] Surko C M and Murphay T 1990 *Phys. Fluid* B **2** 1372
[18] Berezhiani V I, El-Ashry M Y and Mofiz U A 1994 *Phys. Rev.* E **50** 000448
[19] Berezhiani V I and Mahajan S M 1995 *Phys. Rev.* E **52** 001968
[20] Mahajan S M, Berezhiani V I and Miklaszewski R 1998 *Phys. Plasmas* **5** 3264
[21] Eliasson B and Shukla P K 2005 *Phys. Plasmas* **12** 104501
[22] Bulanov S S, Fedotov A M and Pegoraro F 2005 *Phys. Rev.* E **71** 016404
[23] Krall N A and Trivelpiece A W 1973 *Principles of Plasma Physics* (NewYork: McGraw-Hill)
[24] Stix T 1992 *Waves in Plasmas* (New York: American Institute of Physics)
[25] Popel S I, Vladimirov S V and Shukla P K 1995 *Phys. Plasmas* **2** 716
[26] Nejoh Y N 1997 *Aust. J. Phys.* **50** 309
[27] Mahmood S, Mushtaq A and Saleem H 2003 *New J. Phys.* **5** 28.1
[28] Mahmood M A, Mahmood S, Mirza A M and Saleem H 2005 *China. Phys. Lett* **22** 632
[29] Sulem P and Sulem C 1999 *Nonlinear Schrödinger Equation* (Berlin: Springer)
[30] Taniuti T and Yajima N 1969 *J. Math. Phys.* **10** 1369
[31] Asano N, Taniuti T and Yajima N 1969 *J. Math. Phys.* **10** 2020
[32] Kourakis I and Shukla P K 2005 *Nonlinear Proc. Geophys.* **12** 407
[33] Salahuddin M, Saleem H and Saddiq M 2002 *Phys. Rev.* E **66** 036407
[34] Amiranashvili Sh. G and Ignatov A M 1995 *Plasma Phys. Rep.* **21** 364
[35] Kourakis I, Esfandyari-Kalejahi A, Mehdipoor M and Shukla P K 2006 *Phys. Plasmas* **13** 052117
[36] Tsytovich V and Wharton C B 1978 *Commun. Plasma Phys. Cont. Fusion* **4** 91
[37] Fedele R 2002 *Phys. Scr.* **65** 502
Fedele R and Schamel H 2002 *Eur. Phys. J.* B **27** 313